Title
The Influence of the Linker Geometry in Bis(3-hydroxy-N-methyl-pyridin-2-one) Ligands on Solution-Phase Uranyl Affinity

Permalink
https://escholarship.org/uc/item/22d8b3g5

Author
Szigethy, Géza

Publication Date
2011-01-05

Peer reviewed

The Influence of Linker Geometry in bis(3-hydroxy-N-methyl-pyridin-2-one) Ligands on Solution Phase Uranyl Affinity[1]

Dr. Géza Szigethy,[a] *Prof. Dr. Kenneth N. Raymond*[a]*

[a]   Chemical Sciences Division, Lawrence Berkeley National Laboratory, Berkeley, CA 94720 (USA),
        E-mail: raymond@socrates.berkeley.edu
        Fax: (510) 486-5283

        Department of Chemistry, University of California at Berkeley, Berkeley, CA 94720-1460 (USA)

Supporting information for this article is available on the WWW under http://dx.doi.org/10.1002/chem.2010xxxxx. It contains experimental procedures for the synthesis of bis-Me-3,2-HOPO ligands, X-ray diffraction collection and refinement details, conformational analysis of $UO_2(\mathbf{L^9})(DMSO)$, reversibility analyses, UV-visible titration spectra, and speciation diagrams for uranyl titrations. CCDC-783329 contains the supplementary crystallographic data for this paper. These data can be obtained free of charge from The Cambridge Crystallographic Data Centre via www.ccdc.cam.ac.uk/data_request/cif.

Abstract: Seven water-soluble, tetradentate bis(3-hydroxy-N-methyl-pyridin-2-one) (bis-Me-3,2-HOPO) ligands were synthesized that vary only in linker geometry and rigidity. Solution phase thermodynamic measurements were conducted between pH 1.6 and pH 9.0 to determine the effects of these variations on proton and uranyl cation affinity. Proton affinity decreases by introduction of the solubilizing triethylene glycol group as compared to un-substituted reference ligands. Uranyl affinity was found to follow no discernable trends with incremental geometric modification. The butyl-linked 4Li-Me-3,2-HOPO ligand exhibited the highest uranyl affinity, consistent with prior in vivo decorporation results. Of the rigidly-linked ligands, the *o*-phenylene linker imparted the best uranyl affinity to the bis-Me-3,2-HOPO ligand platform.

Introduction

The approach of rational ligand design towards targeted ion chelation seeks to match ligand traits with the geometric and thermodynamic preferences of a target ion.[2] Modifiable ligand properties include ligand geometry, hard/soft character of coordinating atoms, ligand denticity, and geometric pre-organization. Optimization of these design characteristics is observed in bacterial ferric ion shuttling mechanisms,[3, 4] but is also central to synthetic compounds applied in many different selective extraction/removal applications such as heavy metal decorporation,[5, 6] and iron overload treatment.[7-9] Applying rationally-designed ligands towards actinide science is of particularly great interest as nuclear power becomes an attractive carbon-free energy alternative, and the associated risk of environmental and biological exposure to actinides increases.

Unique to the early actinides is the class of linear dioxo cations (actinyls, AnO_2^{n+}) adopted by uranium, neptunium, and plutonium in their +5 or +6 oxidation states. Actinyls pose an unusual challenge to the practice of rational ligand design because, while they display hard Lewis acidity typical of the *f*-elements, they maintain near-linearity in all their known complexes, with the largest distortions of just over 11° occurring only in the presence of very sterically demanding ligands.[10] Unlike most transition metal dioxo cations, ligands coordinate to actinyl cations almost exclusively in a plane perpendicular to the An=O bonds with deviations from this behavior again only occurring in sterically congested complexes.[11] The equatorial coordination plane displays little to no orbital-dictated directionality, with observed coordination geometries ranging from trigonal- through hexagonal-planar, depending on ligand sterics and chelating ability.[12-15] Additionally, the terminal oxo atoms of the actinyl cations (especially in their +6 oxidation state) display poor Lewis basicity, although they have been observed to interact with metal cations in the solid state.[12, 14, 16-20]

The uranyl cation (UO_2^{2+}) is the most common actinyl species studied because uranium is the second most abundant naturally-occuring actinide as well as the one most frequently employed in nuclear power generation.[21] Additionally, the uranyl cation is the most stable form for uranium in oxidizing environments or in vivo. Several different approaches have been used to design uranyl-selective ligands; rigid poly-pyrrole macrocycles have utilized their pre-arranged geometry to form planar uranyl chelates,[22] apically-oriented molecules have introduced Lewis acids in the vicinity of one uranyl oxo

moiety,[23, 24] while some fold-over macrocycles have achieved both these goals simultaneously.[25, 26]

Significant effort has been dedicated towards the development of efficient uranyl cation extraction agents for both analytical and industrial applications, but these studies typically address low pH conditions typical of industrial metal separations technologies.[27, 28] However, the rational development of biological decorporation agents necessarily requires studying the efficacy of uranyl chelation at in vivo pH ranges which are higher than those of industrial/remediation applications. Examples of biologically relevant investigations include that of Czerwinski and co-workers that addresses uranyl speciation with the naturally-occuring siderophore desferrioxamine (DFO)[29] as well as those by Durbin and co-workers that examine the in vivo decorporating ability of poly-bidentate catecholamides and their structural analogs towards the uranyl and transuranic cations.[30-33] These latter studies revealed that 4- or 5-carbon linear linkers provided optimal decorporating ability to poly-bidentate ligands, but the detailed thermodynamic rationale for this result is relatively unexplored.

Recent work in our group has focused on optimizing the equatorial geometric agreement between the uranyl cation and bis(3-hydroxy-N-methyl-pyridin-2-one) (bis-Me-3,2-HOPO) ligands utilizing linker molecules of varying geometries.[34-36] The Me-3,2-HOPO moiety is a bidentate, structural analog to the catecholamide group which binds via hard Lewis basic oxygens and is thus ideal for chelating the strong Lewis-acidic actinide ions. While short linkers best preserve intramolecular hydrogen bonds typical of catecholamide ligands,[36] structural comparisons of the uranyl complexes against that with Pr-Me-3,2-HOPO ($\mathbf{L^1H}$, Figure 1) illustrated that the butyl-linked ligand 4Li-Me-3,2-HOPO provided the most favorable geometry for uranyl chelation of the linearly-linked, tetradentate ligands (nLi-Me-3,2-HOPO, where "n" is the number of carbon atoms in the linker and "Li" stands for "linear").[36] Of the rigidly-linked ligands explored, the 3,4-thiophene, *o*-phenylene, α,α'-*m*-xylene, and 1,8-fluorene linkers (Figure 1) showed the most favorable uranyl coordination geometries; the former two contain very short linkers, while the latter two contain the longest linkers investigated.[35] These results raise the question of whether favorable geometry (optimized in short and long linker lengths) or intramolecular hydrogen bonding (optimized in short linkers) is most important in determining uranyl affinity.

Solution phase titrations were carried out with bis-Me-3,2-HOPO ligands to determine and compare their uranyl affinities. Unfortunately, the bis-Me-3,2-HOPO ligands previously synthesized are not soluble enough in water to enable such measurements, prompting the design and synthesis of water-soluble bis-Me-3,2-HOPO ligands $\mathbf{L^2H_2 - L^8H_2}$ (Figure 2). These ligands incorporate linkers that are structurally analogous to previous ligands, but which also contain a methyl-protected triethyleneglycol moiety to promote water solubility, enabling quantification of their uranyl affinities.

Results and Discussion

Ligand Design and Synthesis. Water solubility was imparted to the bis-Me-3,2-HOPO ligands by introduction of the methyl-protected triethyleneglycol moiety (3,6,9-trioxa-decane) referred to hereon as PEG. This solubilizing group carries no charge in the

pH range investigated here, and thus does not influence the charge of the resultant ligands at varying pH. Uranyl affinity for poly-ether coordination is conveniently poor compared to other neutral Lewis bases, as evidenced by the anhydrous conditions necessary for synthesizing crown-ether inclusion complexes of the uranyl cation.[37] Thus, coordinative interference by the PEG group is unlikely in these titration studies.

However, the location of the PEG substitution is of great concern because it can feasibly affect ligand uranyl affinity in two ways: 1) by inductively influencing the HOPO ring electronics, thereby affecting proton and uranyl affinity of the ligands, and 2) by introducing an additional steric influence, resulting in a solution phase structure significantly different from that seen in prior crystallographic analyses.[35, 36] The Me-3,2-HOPO moiety is inert towards further substitution, relegating PEG substitution to the linker moieties. Due to the extended electronic conjugation in ligands containing 3,4-thiophene and *o*-phenylene linkers (L^6H_2 and L^7H_2), electronic effects on the Me-3,2-HOPO moiety are unavoidable upon substitution at any position on the linker moiety. Such inductive influences will be minimal in the ligands containing the linear nLi- and α,α'-*m*-xylene backbones (L^2H_2 through L^5H_2 and L^8H_2) because the methylene linkers are not conjugated to the Me-3,2-HOPO moieties.

In addition to electronic influences, the potential steric consequences of PEG substitution become significant when the backbone is either small or contains only non-ideal positions upon which to introduce the PEG group. Specifically, steric interference with the amide linkers of the Me-3,2-HOPO moiety is of great concern because intramolecular hydrogen bonding involving the amide proton is a significant interaction in HOPO and more generally in catecholamide ligands.[38] Of particular concern is substitution on the 3,4-thiophene linker, which is relegated only to the 2- and 5-positions, the steric consequence of which is the formation of dimers of the form $[UO_2L_2(solv.)]_2$ as opposed to the mononuclear uranyl species seen with the unsubstituted 3,4-thiophene-bis-Me-3,2-HOPO ligand.[34] Because the available substitution positions on the 2Li linker are adjacent to the linking amides and cannot avoid some influence on the proton and/or uranyl affinity in L^2H_2, the PEG moiety was introduced at the same position on the 3Li, 4Li, and 5Li linkers to make affinity comparisons at least internally consistent between ligands $L^2H_2 - L^5H_2$.

Substitution on the α,α'-*m*-xylene backbone in L^8H_2 contains perhaps the most ideal PEG location of the ligands investigated. Firstly, the PEG moiety is located four carbons from the linking amide nitrogens, ensuring minimal steric effects, and secondly, the PEG group is electronically isolated from the HOPO moieties due to the presence of the methylene spacers between the phenyl ring and the HOPO amides. Thus, it is expected that the behavior of ligand L^8H_2 in solution will most closely resemble that of its unsubstituted analog compared to the other PEG-bis-Me-3,2-HOPO ligands.

Absent from the backbones illustrated in Figure 2 is the 1,8-fluorene moiety that was shown to provide a very good geometric match to the uranyl cation coordination preferences while displaying a degree of ligand pre-organization.[35] Unfortunately, the tremendous insolubility imparted on bis-Me-3,2-HOPO ligands by the fluorene backbone cannot be undone by solubilizing group substitution due to synthetic impracticality and the natural electrophillic substitution behavior of fluorene and its structural analog

dibenzofuran; thus a soluble 1,8-diaminofluorene-linked bis-Me-3,2-HOPO ligand was not pursued.

Structural Consequence of PEG Substitution in L^7H_2. The geometric and electronic consequences of PEG substitution on the 3,4-thiophene and *o*-phenylene linkers must be addressed due to the extended conjugation possible through the aromatic linkers. Thioalkyl substitution on the 3,4-thiophene linker in bis-Me-3,2-HOPO ligands is know to result in sterically-induced $[UO_2(L)(solv.)]_2$ dimer formation,[34] a behavior that ligand L^8H_2 will certainly duplicate. In contrast, the PEG groups in L^7H_2 are *meta* to the amide nitrogens, and the ligand is thus expected to maintain planarity upon uranyl chelation, with the resultant conjugation allowing for a potentially increased inductive influence by the PEG substitution. To investigate the presence/severity of such an effect, the propoxy-substituted ligand L^9H_2 and its uranyl complex were synthesized (Figure 3). Crystallographic parameters for this structure are listed in Table 1.

The $UO_2(L^9)(DMSO)$ crystal structure displays the expected mononuclear speciation seen with other bis-Me-3,2-HOPO ligands,[35, 36] with a pentagonal planar uranyl coordination geometry provided on four points by $(L^9)^{2-}$, and a fifth site occupied by a DMSO oxygen. Significantly, the propoxy substituents are situated away from the amide linkers, so it can be assumed that PEG groups in L^7H_2 will not impart significant steric influence on the resultant uranyl complex. The equatorial $U–O_{phenol}$ and $U–O_{amide}$ bond lengths are 2.34(1) Å and 2.42(2) Å, respectively, which are statistically identical to the similar equatorial U–O bond lengths in the uranyl complex with the unsubstituted *o*-phenylene-Me-3,2-HOPO ligand.[35] As Figure 3 illustrates, the backbone aryl group is not co-planar with the HOPO moieties due to a torsion in the linking amide moieties. The $C_{ring}–N_{amide}$ torsion angles of 156° and 167° presumably relieve a potential close contact between the amide protons in the metal-chelating form that is observed to a similar extent in the unsubstituted uranyl complex (torsions of 148° and 157°),[35] as well as in the Eu(III) complex with the structurally-similar *o*-phenylene-1,2-HOPO ligand (torsions of 157°, 159°, and 169°).[39] Thus, while there are slight differences in the co-planarity of the $UO_2(L^9)(DMSO)$ crystal structure from its unsubstituted complex (see Supporting Information), the overall structure is similar to that with its unsubstituted analog.

To assess the potential electronic effect of PEG substitution on the *o*-phenylene linker in L^7H_2 the ^1H NMR resonances of the amide protons in free L^9H_2 and its uranyl complex can be compared against those in the unsubtituted *o*-phenylene-Me-3,2-HOPO ligand and its uranyl complex.[35] The amide proton chemical shifts of free L^9H_2 are 0.13 ppm upfield of that in *o*-phenylene-Me-3,2-HOPO, suggesting some electronic donation into the aryl linker upon alkoxy substitution. However, these same resonances are only 0.06 ppm upfield of the unsubstituted ligand once coordinated to the uranyl cation. The similarity in these values suggests that the inductive effects of alkoxy substitution on the 3- and 4-positions of the *o*-phenylene linker are minor, especially upon uranyl chelation. Additionally, the amide chemical shifts in L^7H_2 are 0.01 ppm shifted from L^9H_2, indicating a near-identical inductive effect. The crystallographic and NMR comparisons thus indicate that the PEG substitution in L^7H_2 should have a relatively insignificant impact on the resultant uranyl complex geometry either through steric or inductive processes.

Solution Thermodynamics. In the presence of dissolved metal ion (M^{a+}) and protonated ligand (LH_n, where L is a ligand with *n* removable protons), a pH-dependent metal-ligand complex of general formula $M_mL_lH_h$ forms according to the equilibrium shown in Equation 1. The relative amount of each species in solution is determined by Equation 2, the rearrangement of which provides the standard formation constant notation of $\log \beta_{mlh}$ (Equation 3). The $\log \beta_{mlh}$ value describes a cumulative formation constant, but a stepwise formation constant ($\log K$) can be calculated from $\log \beta_{mlh}$ values using Equation 4. When addressing protonation constants, the stepwise formation constants are commonly reported as dissociation constants ($-\log K$, or pK_a).

Eq. 1: $m M^{a+} + l L^{b-} + h H^+ \xrightleftharpoons{\beta_{mlh}} M_mL_lH_h^{(ma-lb+h)+}$
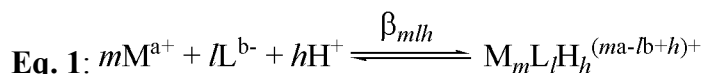
Eq. 2: $[M_mL_lH_h] = \beta_{mlh}([M]^m[L]^l[H]^h)$

Eq. 3: $\log \beta_{mlh} = \log \{([M_mL_lH_h])/([M]^m[L]^l[H]^h)\}$

Eq. 4: $\log K_{01n} = \log\{([LH_n])/([LH_{n-1}][H])\} = \log \{(\beta_{01n}/\beta_{01(n-1)}\} = \log \beta_{01n} - \log \beta_{01(n-1)}$

Because bis-Me-3,2-HOPO ligands are diprotic and require deprotonation for metal chelation, their affinity for any metal is necessarily pH dependent (Scheme 1). Although the most common pH for biological applications is that of blood serum, or pH 7.4, it is also desirable to investigate the uranyl affinity of bis-Me-3,2-HOPO ligands in acidic and caustic media, as such conditions are encountered in industrial or storage tank waste remediation applications.[40, 41]

Proton Titrations/Affinity. Protonation constants of ligands $\mathbf{L^2H_2} - \mathbf{L^8H_2}$ were determined using potentiometric titrations at about 150-200 μM ligand concentration. As a point of comparison for ligands $\mathbf{L^2H_2} - \mathbf{L^5H_2}$, the protonation constants for the previously reported 2Li- and 4Li-Me-3,2-HOPO ligands[36] were also measured, but were performed spectrophotometrically due to their lower solubility at about 50 μM ligand concentration. A 5% starting DMSO concentration in all protonation titrations was required for consistency with uranyl titration conditions. Data were analyzed as described in the Experimental Section and the resultant pK_a values are listed in Table 2. The sum of the pK_a values (ΣpK_a) is also listed, which corresponds to the $\log \beta_{012}$ formation constant and is a general measure of ligand acidity, with lower ΣpK_a values indicating a more acidic ligand.

One trend visible in Table 2 is that linearly-linked ligands with shorter linkers (smaller *n*) have lower ΣpK_a values than those with longer linkers. This general trend is seen in ligands $\mathbf{L^2H_2} - \mathbf{L^5H_2}$ ($\Delta\Sigma pK_a \approx 0.7$) as well as between 2Li- and 4Li-Me-3,2-HOPO ($\Delta\Sigma pK_a \approx 0.5$). A second trend is that substitution of the PEG moiety on the linear linkers via an amide linker also lowers the ΣpK_a compared to the unsubstituted ligands, as evidenced by comparing 2Li-Me-3,2-HOPO against $\mathbf{L^2H_2}$ ($n = 2$) and 4Li-Me-3,2-HOPO against $\mathbf{L^4H_2}$ ($n = 4$). This latter trend is primarily caused by a drop in pK_{a1} ($\Delta pK_{a1, max} \approx 0.7$), but also affects the pK_{a2} values ($\Delta pK_{a2, max} \approx 0.4$). The drop in ΣpK_a upon PEG substitution ($\Delta\Sigma pK_a/PEG \approx 1.1$) is more significant than that accompanying

incremental shortening of the linker lengths (average $\Delta\Sigma pK_a/n \approx 0.23$). However, in both these trends, it can be assumed that the decrease in pK_a arises from enhanced stabilization of the deprotonated phenolate oxygen, since the electronics of the HOPO moiety remain roughly constant in ligands $\mathbf{L^2H_2} - \mathbf{L^8H_2}$.

The intramolecular hydrogen bond stabilization of phenolates by *ortho* amide protons are well established and is illustrated in Figure 4(a) as it applies to Me-3,2-HOPO moieties.[38] However, the trends observed in Table 2 suggest that additional hydrogen bond interactions become significant upon shortened linker length (smaller *n*) or PEG moiety introduction. The drop in pK_{a1} associated with shortened linker length can be explained by an increased proximity of the second amide group to the initially deprotonated phenolate group as shown in Figure 4(b), which applies in both the unsubstituted and PEG-functionalized nLi-Me-3,2-HOPO ligands. Similarly, the drop in pK_{a1} upon PEG-functionalization is most likely caused by hydrogen bond donation from the PEG-amide nitrogen, as illustrated in Figure 4(c). This latter stabilization from the PEG-amide group in ligands $\mathbf{L^2H_2} - \mathbf{L^5H_2}$, while unintended, can be considered roughly constant due to the identical location of the PEG-amide group in the linear backbone linkers. Thus, the electronic and geometric effects of linker length can be considered to be the prominent trend observed in titrations with PEG-nLi-Me-3,2-HOPO ligands.

The pK_a values for ligands $\mathbf{L^6H_2} - \mathbf{L^8H_2}$ cannot be compared against their PEG-free versions due to the latter's poor solubility in aqueous media. However, the PEG moiety in ligands $\mathbf{L^6H_2}$ and $\mathbf{L^7H_2}$ is expected to have some inductive influence on proton affinity, since in free $\mathbf{L^6H_2}$ and $\mathbf{L^7H_2}$ the amide ^{1}H NMR resonances are shifted upfield by 0.29 ppm and 0.08 ppm, respectively, as compared to their unsubstituted analogs.[35] This inductive influence is obviously much larger in $\mathbf{L^6H_2}$ than in $\mathbf{L^7H_2}$, but the steric consequences of 2,5-disubstitution on the thiophene linker are known to be significant,[43] so the inductive effect is presumed to be of minor importance in ligand $\mathbf{L^6H_2}$ upon uranyl chelation. In contrast, $\mathbf{L^8H_2}$ is expected to experience very little steric or electronic influences by PEG moiety inclusion, and indeed has a ΣpK_a very similar to that of $\mathbf{L^5H_2}$, which is also an *n* = 5 ligand.

Uranyl Titrations/Affinity. The uranyl affinities of ligands $\mathbf{L^2H_2}$ through $\mathbf{L^8H_2}$ were determined by performing spectrophotometric titrations. The poor solubility of the uranyl complexes necessitated 5 μM analyte concentrations as well as a 5% starting DMSO concentration to assist in solvating the neutral uranyl complexes at neutral pH. Unfortunately, uranyl titrations with ligands 2Li-Me-3,2-HOPO, 4Li-Me-3,2-HOPO, and $\mathbf{L^9H_2}$ are impossible even at these low concentrations due to slow and reversible precipitation of a neutral $UO_2(L)(solv.)$ species near neutral pH. The bidentate ligand Pr-Me-3,2-HOPO was found to be sufficiently soluble for spectrophotometric titrations at these concentrations. Metal-to-ligand ratios used in the titrations were those observed in the crystal structures of the uranyl complexes with unsubstituted Me-3,2-HOPO ligands, namely 1:1 for bis-Me-3,2-HOPO ligands and 1:2 for Pr-Me-3,2-HOPO. Three independent titrations were measured between pH 2.4 and 11.0 except where reversibility analysis indicated a point in the titrations beyond which the complexes underwent an irreversible chemical change. Because the uranyl complexes routinely form below pH 4, two strong acid titrations (pH 3.0 to 1.6) were carried out for each ligand.

The uranyl titration spectra with PEG-substituted bis-Me-3,2-HOPO ligands generally exhibited similar absorption spectra in the range of 250-400 nm, with a large absorption maximum in the 330–350 nm range, and often with a subtle shoulder at longer wavelengths. These absorption features closely resemble those of the free ligands, and are thus attributed to $\pi \rightarrow \pi^*$ transitions. Titrations with $\mathbf{L^6H_2}$ exhibited the most unusual spectrum investigated, with a broad absorption feature in the 275–300 nm range, at which the other bis-Me-3,2-HOPO ligands display absorption minima. Independent of absorption features, however, absorption maxima with all ligands red shift upon increasing pH, corresponding to deprotonation/metallation of the ligand. Although the uranyl complexes with bis-Me-3,2-HOPO ligands are red or orange in the solid state and in concentrated solution, no significant absorption transition was observed in wavelengths above 400 nm at 5 μM concentrations.

Most uranyl titrations were reversible through the highest pH ranges of the titrations (typically pH 11.0–11.4), indicating that no unforeseen chemical changes occur in the metal-ligand complex in solution (Figure 5). In contrast, titrations with fully-conjugated ligands $\mathbf{L^6H_2}$ and $\mathbf{L^7H_2}$ exhibited poor reversibility when titrations were taken to pH 11.0 (Figure 5). It was found that running the titrations only up to pH 8.5 and 9.0, respectively, restored reversibility in the uranyl titrations. The cause of this irreversibility is unknown, but corresponds roughly to additional deprotonation of or continued hydroxide introduction to the $[UO_2(L)(OH)]^-$ complex to form a $[UO_2(L)H_{-2}]^{2-}$ species (where H_{-1} represents hydroxide coordination or incremental complex deprotonation). To maintain consistency across the various bis-Me-3,2-HOPO ligands, titration data were truncated before the onset of the $[UO_2(L)H_{-2}]^{2-}$ species. For most ligands, this data truncation occurred at about pH 9.0. Complete titration figures are provided in the Supporting Information.

Uranyl titrations with all Me-3,2-HOPO ligands displayed a rapid increase in intensity between pH 2 and pH 4, indicating deprotonation of the ligand and complexation of the uranyl cation. For tetradentate ligands (with the exception of $\mathbf{L^6H_2}$), this result was refined as the formation of a $UO_2L(solv.)$ complex. This assumption requires the simultaneous deprotonation of both Me-3,2-HOPO moieties, but is reasonable considering the similarity between pK_{a1} and pK_{a2} of these ligands and because uranyl chelation will drive deprotonation of a chelating ligand at lower pH.[44] The UV-visible spectra shifted again around neutral pH, which was refined as the formation of a $[UO_2L(OH)]^-$ species (Scheme 2). This partial hydrolysis occurs near neutral pH because the fifth equatorial coordination position on the uranyl is known to be occupied by solvent in bis-Me-3,2-HOPO complexes,[35, 36] and thus hydroxide coordination does not necessitate ligand displacement. A similar partial hydrolysis event is observed in the uranyl complex with the potentially hexadentate desferrioxamine B (DFO), in which a $[UO_2(DFO)(OH)]^-$ complex was observed to form at neutral pH.[29]

Because 2,5-disubstituted thiophene-Me-3,2-HOPO ligands form dimeric $[UO_2(L)(solv.)]_2$ complexes,[34] such dimeric species were required in the refinement of titration data with $\mathbf{L^6H_2}$. Refinement of the strong acid titration data was attempted two ways, assuming either that a mononuclear species $[UO_2(\mathbf{L^6})H_{0/1}]^{0/+}$ forms before a $[UO_2(\mathbf{L^6})(solv.)]_2$ dimer, or that the dimer forms in a concerted fashion, but only the latter strategy led to stable data refinement. This behavior suggests that the substitution on the

thiophene ligand inhibits mononuclear complex formation even at the low concentrations used, which prior crystallographic studies led us to expect.[34] Because both uranyl cations in the solid state $[UO_2(L)(solv.)]_2$ dimer crystal structure displayed pentagonal planar coordination with one site occupied by solvent, the titration data were refined such that the $[UO_2(\mathbf{L^6})(solv.)]_2$ dimer experiences two partial hydrolysis events, forming first a $\{[UO_2(\mathbf{L^6})(solv.)][UO_2(\mathbf{L^6})(OH)]\}^-$ species, followed by a $\{[UO_2(\mathbf{L^6})(OH)]_2\}^{2-}$ species (Scheme 3). The onset of titration irreversibility at pH 8.0 coincides with hydrolysis beyond the $\{[UO_2(\mathbf{L^6})(OH)]_2\}^{2-}$ species and is consistent with the onset of irreversibility in the uranyl titrations with $\mathbf{L^7H_2}$ which was observed upon hydrolysis/deprotonation beyond the formation of the $[UO_2(\mathbf{L^7})(OH)]^-$ species.

The speciation of uranyl complexes with bidentate $\mathbf{L^1H}$ in solution are necessarily very different from those with $\mathbf{L^2H_2} - \mathbf{L^8H_2}$. Because $\mathbf{L^1H}$ has only one proton, $\mathbf{L^1}$ binds the uranyl cation at very low pH to first form a $[UO_2(\mathbf{L^1})(solv.)_x]^+$ complex which is the major species until pH 5.5, when the $UO_2(\mathbf{L^1})_2(solv.)$ complex observed in crystal structure analysis[36] becomes the dominant species. This complex first undergoes the expected partial hydrolysis to form $[UO_2(\mathbf{L^1})_2(OH)]^-$, then experiences one more hydrolysis below pH 10. This last hydrolysis product could be refined as either a $[UO_2(\mathbf{L^1})H_{-2}]^-$ or $[UO_2(\mathbf{L^1})_2H_{-2}]^{2-}$ species, with near negligible changes in the other formation constants. The former corresponds to displacement of one ligand upon coordination of a second hydroxide, while the latter corresponds to either deprotonation of a coordinated ligand or the introduction of hydroxide to the uranyl coordination plane without ligand displacement. The lack of acidic protons on coordinated Me-3,2-HOPO moieties rules out the possibility of additional deprotonation. However, the coordination of additional hydroxide would crowd the uranyl coordination plane, and the low concentrations and 1:2 UO_2:$\mathbf{L^1H}$ ratios used in the titrations suggest that ligand displacement to form a $[UO_2(\mathbf{L^1})(OH)_2]^-$ species at high pH is the more likely speciation in these titrations (Scheme 4).

Titration data analysis using the speciation models described above yielded the formation constants listed in Table 3. Because log β_{mlh} values are species dependent, with each ligand displaying different pK_a values and uranyl complexation behavior, a species-independent method is needed to compare uranyl affinities. A metric frequently used for this purpose is that of pM (for this study pUO_2) where $pUO_2 = -\log[UO_2^{2+}{}_{free}]$, and "$UO_2^{2+}{}_{free}$" refers to solvated uranyl ion free of complexation by ligand or hydroxide. Using this metric, higher pUO_2 values correspond to a lower concentration of uncomplexed uranyl in solution. pUO_2 is calculated using standard conditions of $[UO_2^{2+}] = 10^{-6}$ M and $[L] = 10^{-5}$ M (L:UO_2^{2+} = 10), and thus the minimum pUO_2 value is 6.0, at which no metal complexation occurs. While typically reported at physiological pH, pUO_2 can be calculated at any pH once proton and uranyl affinities are known; pUO_2 values at pH 2.5, 7.4 and 8.5 are listed for each Me-3,2-HOPO ligand in Table 4.

The pUO_2 values in Table 4 reveal that the uranyl affinity of bis-HOPO ligands does indeed vary with changes in ligand geometry. However, the affinities do not follow gradual trends of the sort observecd in Table 2, where linker length and degree of conjugation affected ligand proton affinity in an incremental fashion. In contrast, small changes in linker length and geometry resulted in large changes in pUO_2, with no noticeable correlation with the physical metrics gleaned from crystal structure

analysis.[35] Common to all ligands, however, is a dramatic rise in pUO$_2$ (about 7 log units) between pH 2.5 and pH 7.4. It is not possible to credit this pUO$_2$ increase entirely to a rise in ligand affinity, because concentrations of uranyl hydrolysis products $[(UO_2)_m(OH)_n]^{(2m-n)+}$ increase upon increased pH, lowering $[UO_2^{2+}_{free}]$ independent of ligand identity or efficacy. However, because Me-3,2-HOPO ligands require deprotonation for metal chelation, it is reasonable to suspect that the majority of this rise in pUO$_2$ comes from a change in ligand affinity upon complete deprotonation at higher pH. This assumption is also supported by the UV-visible titration spectra, which exhibit significant shifts in λ_{max} and absorption intensity upon increasing pH from 2.5 to 7.4, suggesting increased ligand chelation of the uranyl cation.

Focusing on ligands **L^{2}H$_2$** – **L^{5}H$_2$**, there is no trend in uranyl affinity upon incremental increase in linker length at any pH. Because ligand pK$_a$ decreases as linker length shortens, **L^{2}H$_2$** would be expected to bind most strongly to the uranyl cation. However, **L^{2}H$_2$** displays the second highest affinity, with **L^{4}H$_2$** displaying the strongest uranyl affinity at both low and high pH. **L^{4}H$_2$** has a higher ΣpK$_a$ than both **L^{2}H$_2$** and **L^{3}H$_2$**, so the observed uranyl affinity must be due to geometry effects. This high affinity is consistent with the relatively relaxed geometry observed in the UO$_2$(4Li-Me-3,2-HOPO)(DMSO) crystal structure as well as with the superior ability for 4Li-Me-3,2-HOPO to chelate actinides in vivo.[31, 36]

Of the rigidly-linked ligands **L^{6}H$_2$** – **L^{8}H$_2$**, **L^{6}H$_2$** is the most acidic, and yet displays the poorest uranyl affinity at all pH. This may be due to the inability to form monomeric uranyl complexes. The low pUO$_2$ of **L^{6}H$_2$** at higher pH is presumed to be a geometric effect caused by the amide rotation necessitated by substitution at the 2- and 5-positoins of the thiophene ring.[34] Unfortunately, such distortions are unavoidable in solubilized 3,4-thiophene-Me-3,2-HOPO ligands, and whether similar uranyl affinities would be observed in geometrically similar, less sterically-congested, N-substituted 3,4-pyrrole-Me-3,2-HOPO ligands remains a question for future study.

Ligand **L^{7}H$_2$** shows the most favorable pUO$_2$ of the rigidly-linked ligands, approaching that of **L^{4}H$_2$**. Because minor pK$_a$ changes are apparently not a significant factor in determining uranyl affinity in bis-Me-3,2-HOPO ligands, this affinity is presumably due to a favorable geometric agreement between the ligand and the uranyl coordination preferences. The pUO$_2$ of **L^{7}H$_2$** is also higher than that of **L^{2}H$_2$** (both $n = 2$), indicating that ligand rigidity and appropriate preorganization favor high uranyl affinity, as expected. In contrast, the pUO$_2$ of **L^{8}H$_2$** is significantly lower, despite the favorable conformational parameters observed in crystal structures of the unsubstituted UO$_2$(*m*-xy-Me-3,2-HOPO)(DMF) structure.[35]

The high pUO$_2$ of **L^{1}H**, which rivals that of **L^{4}H$_2$** at pH 2.5 and **L^{2}H$_2$** at high pH, can be understood by considering that uranyl chelation by **L^{1}H** at low pH requires a single deprotonation event, while chelation of bis-Me-3,2-HOPO ligands requires two, making $(\mathbf{L^1})^-$ coordination relatively favorable at low pH. At high pH, the speciation model with **L^{1}H** also reveals that the relatively high affinity is accompanied by ligand displacement in favor of hydroxide ion. Thus, although **L^{1}H** exhibits a high pUO$_2$, the individual Pr-Me-3,2-HOPO ligands display significantly less affinity towards the uranyl cation than the bis-Me-3,2-HOPO ligands, as the chelate effect would lead one to expect.

Conclusions

Seven PEG-substituted bis-Me-3,2-HOPO ligands were synthesized as water-soluble, structural analogs to ligands subjected to prior crystallographic analysis.[35, 36] Solution thermodynamic measurements demonstrated that linker length and geometry have a measurable effect on the proton affinity of bis-Me-3,2-HOPO ligands, but that uranyl affinity of these ligands does not correlate with trends in proton affinity. Significantly, the PEG-4Li-Me-3,2-HOPO ligand L^4H_2 bound most strongly to the uranyl cation, which supports earlier observations from in vivo chelation studies and crystallographic studies.[32, 36] The *o*-phenylene linker in L^7H_2 imparted the second highest uranyl affinity, rivaling that of L^4H_2, and had a higher affinity than the similarly-sized L^2H_2. Because these results are generally independent of ligand acidity, it can be concluded that ligand geometry imparted by the linker structure (and perhaps ligand preorganization in the case of L^7H_2) is responsible for the observed uranyl affinities.

One aspect the uranyl titrations and the resultant pUO_2 values described above do not address is the matter of selectivity. In most applications associated with biological removal of actinides, high binding constants are necessary, but high selectivity is also desirable if an administered drug is to be effective. Such selectivity is also necessary in industrial extraction processes, so further evaluation of bis-Me-3,2-HOPO ligands will require titration measurements against biologically relevant ions such as Ca^{2+} and Zn^{2+}, as well as other actinides.

Experimental Section

Titration Solutions and Equipment. Corning high performance combination glass electrodes (response to [H$^+$] was calibrated before each titration[45]) were used together with either an Accumet pH meter or a Metrohm Titrino to measure the pH of the experimental solutions. Metrohm autoburets (Dosimat or Titrino) were used for incremental additions of acid or base standard solution to the titration cell. The titration instruments were fully automated and controlled using LabVIEW software.[46] Titrations were performed in 0.1 M KCl supporting electrolyte under positive Ar gas pressure. The temperature of the experimental solution was maintained at 25 °C by an externally circulating water bath. UV-visible spectra for incremental titrations were recorded on a Hewlett-Packard 8452a spectrophotometer (diode array). Solid reagents were weighed on a Metrohm analytical balance accurate to 0.01 mg. All titration solutions were prepared using distilled water that was purified by passing through a Millipore Milli-Q reverse osmosis cartridge system and degassed by boiling for 1 h while being purged under Ar. Carbonate-free 0.1 M KOH was prepared from Baker Dilut-It concentrate and was standardized by titrating against potassium hydrogen phthalate using phenolphthalein as an indicator. Solutions of 0.1 M HCl were similarly prepared and were standardized by titrating against sodium tetraborate decahydrate to Methyl Red endpoint. Ligand stock solutions were made by dissolving a weighed amount of ligand accurate to 0.01 mg in DMSO in a volumetric flask. These stock solutions were frozen when not in use to prevent ligand decomposition. A stock uranyl solution in 1.2 wt% nitric acid was purchased from Aldrich (4.22 mM) and used as received. UO_2:L ratios were controlled by careful addition of uranyl and ligand solutions to the titration vessel.

Spectrophotometric and Potentiometric Titrations: All titrations were performed with about 5% starting concentration of DMSO added to the KCl solution to promote the solvation of protonated ligands and their neutral uranyl complexes. Spectrophotometric titrations were carried out in the presence of 10-20 equivalents (as compared to ligand concentration) of NH_4Cl, MES, and HEPES buffers in order to dampen the pH change between incremental additions of titrant. Each addition of acid or base was followed by an equilibration period before pH and absorbance data were collected. For potentiometric titrations this delay was 300 seconds and for spectrophotometric titrations was 600 seconds for free ligand and 600-1200 seconds for titrations in the presence of UO_2^{2+}. Spectra were recorded between 250-550 nm. The UV-silent region above 420 nm was monitored for baseline drift as an indication of precipitated material.

Potentiometric titrations were carried out at 150-200 μM ligand concentrations. Spectrophotometric titrations for protonation constants of 2Li-Me-3,2-HOPO and 4Li-Me-3,2-HOPO were carried out at about 50 μM ligand concentrations using a titration cell with a 1 cm path length quartz cuvette attached. Spectrophotometric titrations for uranyl affinity were performed at about 6 μM complex concentration using a 6.6 cm path length quartz-windowed titration cell. All mid-pH titrations were repeated a minimum of three times and were run forwards and backwards (from acid to base and reverse) within limits set by the reversibility of the titration.

Spectrophotometric uranyl titrations of L^2H_2 – L^8H_2 were performed at approximately 5 μM concentrations using a 6.6 cm path length quartz-windowed titration cell with a 5% starting DMSO concentration necessary for complete salvation of neutral uranyl species near neutral pH. Three independent titrations, each consisting of a forward (acid to base) and reverse (base to acid) titration, were measured between pH 2.4 and 11.0 except where reversibility analysis indicated a point in the titrations beyond which the complexes underwent an irreversible chemical change. Low pH titrations were performed from pH 3 down to pH 1.6, and electrodes were calibrated as described in a previous publication.[47]

Titration Data Treatment: Potentiometric data were analyzed using Hyperquad[48, 49] software. The data from at least three independent titrations, each consisting of one forward (pH 3 to pH 10) and one reverse (pH 10 to pH 3) titration were analyzed separately. These analyses resulted in similar values, so were refined together to provide better fit statistics. Spectrophotometric titration data were analyzed using the program pHab.[50] Data from three independent titrations consisting of one forward and one reverse titration were analyzed separately, with the forward and backward runs refined separately. Both analysis programs utilized nonlinear least squares regression to determine formation constants.

Values for the hydrolysis product of the uranyl cation were taken from a recent literature publication.[51] Wavelengths between 250-400 nm were typically used for data refinement of spectrophotometric titrations. The number of absorbing species to be refined upon was determined by factor analysis within the pHab program suite.[50] Reversibility of spectrophotometric titrations was determined by comparison of the species- and concentration-independent value A*v (absorbance*volume) at selected wavelengths for the forward and reverse titrations. Speciation diagrams were generated using HYSS2[52, 53] titration simulation software and the protonation and metal complex

formation constants were determined by potentiometric and spectrophotometric titration experiments.

[1]   This paper is #62 in the series "Specific Sequestering Agents for the Actinides." For the previous paper, see reference number 35.

[2]   É. Ansoborlo, B. Amekraz, C. Moulin, V. Moulin, F. Taran, T. Bailly, R. Burgada, M.-H. Hengé-Napoli, A. Jeanson, C. Den Auwer, L. Bonin, P. Moisy, *C. R. Chemie* **2007**, *10*, 1010-1019.

[3]   S. I. Müller, M. Valdebenito, K. Hantke, *Biometals* **2009**, *22*, 691-695.

[4]   M. A. Fischbach, H. Lin, D. R. Liu, C. T. Walsh, *Nature Chem. Bio.* **2006**, *2*, 132-138.

[5]   O. Andersen, *Chem. Rev.* **1999**, *99*, 2683-2710.

[6]   D. F. Back, É. Bonfada, M. Manzoni de Oliveira, E. S. Lang, *J. Inorg. Biochem.* **2007**, *101*, 709-714.

[7]   M. D. Cappellini, P. Patoneri, *Annu. Rev. Med.* **2009**, *60*, 25-38.

[8]   R. C. Hider, *Biochem. Soc. Trans.* **2002**, *30*, 751-754.

[9]   G. J. Kontoghiorghes, K. Neocleous, A. Kolnagou, *Drug Safety* **2003**, *26*, 553-584.

[10]   J. Maynadié, J.-C. Berthet, P. Thuery, M. Ephritikhine, *Chem. Comm.* **2007**, 486-488.

[11]   J.-C. Berthet, P. Thuery, J.-P. Dognon, D. Guillaneux, M. Ephritikhine, *Inorg. Chem.*, *47*, 6850-62.

[12]   C. J. Burns, D. L. Clark, R. J. Donohoe, P. B. Duval, B. L. Scott, C. D. Tait, *Inorg. Chem.* **2000**, *39*, 5464-5468.

[13]   N. N. Rammo, K. R. Hamid, T. K. Ibrahim, *J. Alloys. Compd.* **1994**, *210*, 319-324.

[14]   M. J. Sarsfield, M. Helliwell, J. Raftery, *Inorg. Chem.* **2004**, *43*, 3170-3179.

[15]   D. H. Templeton, A. Zalkin, H. Ruben, L. K. Templeton, *Acta Cryst. C* **1985**, *C41*, 1439-1441.

[16]   P. Thuéry, B. Masci, M. Takimoto, T. Yamato, *Inorg. Chem. Comm.* **2007**, *10*, 795-799.

[17]   W. Zhang, J. Zhao, *Inorg. Chem. Comm.* **2006**, *9*, 397-399.

[18]   B. Masci, P. Thuéry, *Cryst. Eng. Comm.* **2007**, *9*, 582-590.

[19]   J. A. Danis, M. R. Lin, B. L. Scott, B. W. Eichhorn, W. H. Runde, *Inorg. Chem.* **2001**, *40*, 3389-3394.

[20]   P. Thuéry, B. Masci, *J. Chem. Soc. Dalton Trans.* **2003**, 2411-2417.

[21]   I. Grenthe, J. Drozdzynski, T. Fujino, E. C. Buck, T. E. Albrecht-Schmitt, S. F. Wolf, in *The Chemistry of the Actinide and Transactinide Elements, Vol. 1*, 3rd ed.

(Eds.: L. R. Morss, N. M. Edelstein, J. Fuger), Springer, Dordrecht, The Netherlands, **2006**, pp. 253-698.

[22] J. L. Sessler, D. Seidel, A. E. Vivian, V. Lynch, B. L. Scott, D. W. Keogh, *Angew. Chem. Int. Ed.* **2001**, *40*, 591-594.

[23] T. S. Franczyk, K. R. Czerwinski, K. N. Raymond, *J. Am. Chem. Soc.* **1992**, *114*, 8138-8146.

[24] P. H. Walton, K. N. Raymond, *Inorg. Chim. Acta.* **1995**, *240*, 593-601.

[25] P. L. Arnold, A. J. Blake, C. Wilson, J. B. Love, *Inorg. Chem.* **2004**, *43*, 8206-8208.

[26] P. L. Arnold, D. Patel, A. J. Blake, C. Wilson, J. B. Love, *J. Am. Chem. Soc.* **2006**, *128*, 9610-9611.

[27] J. N. Mathur, M. S. Murali, K. L. Nash, *Solv. Extr. Ion Exch.* **2001**, *19*, 357-390.

[28] A. P. Paiva, P. Malik, *J. Radioanal. Nucl. Chem.* **2004**, *261*, 485-496.

[29] L. Mullen, C. Gong, K. R. Czerwinski, *J. Rad. Nucl. Chem.* **2007**, *273*, 683-688.

[30] P. W. Durbin, *Health Phys.* **2008**, *95*, 465-492.

[31] P. W. Durbin, B. Kullgren, S. N. Ebbe, J. Xu, K. N. Raymond, *Health Phys.* **2000**, *78*, 511-521.

[32] P. W. Durbin, B. Kullgren, K. N. Raymond, *Rad. Prot. Dosim.* **1998**, *79*, 433-443.

[33] A. E. V. Gorden, J. Xu, K. N. Raymond, *Chem. Rev.* **2003**, *103*, 4207-4282.

[34] G. Szigethy, K. N. Raymond, *Inorg. Chem.* **2009**, *48*, 11489-11491.

[35] G. Szigethy, K. N. Raymond, *Inorg. Chem.* **2010**, *49*, 6755-6765.

[36] J. Xu, K. N. Raymond, *Inorg. Chem.* **1999**, *38*, 308-315.

[37] P. Thuéry, N. Keller, M. Lance, J. D. Figner, M. Nierlich, *New J. Chem.* **1995**, *19*, 619-625.

[38] T. M. Garrett, M. E. Cass, K. N. Raymond, *J. Coord. Chem.* **1992**, *25*, 241-253.

[39] A. D'Aléo, J. Xu, E. G. Moore, C. J. Jocher, K. N. Raymond, *Inorg. Chem.* **2008**, *47*, 6109-6111.

[40] (Ed.: N. R. Council), National Research Council, Washington, DC, **2000**, p. 142.

[41] (Ed.: N. R. Council), National Research Council, Washington, DC, **2001**, p. 198.

[42] J. Xu, P. W. Durbin, B. Kullgren, K. N. Raymond, *J. Med. Chem.* **1995**, *38*, 2606-2614.

[43] G. Szigethy, K. N. Raymond, *Inorg. Chem.* **2009**, *48*, 11489-91.

[44] Z. Szabó, I. Grenthe, *Inorg. Chem.* **2000**, *39*, 5036-5043.

[45] P. Gans, B. O'Sullivan, *Talanta* **2000**, *51*, 33-37.

[46] *LABVIEW, version 8.0; National Instruments Corp.: 11500 N Mopac Expwy, Austin, TX 78759-3504*.

[47] A. R. Johnson, B. O'Sullivan, K. N. Raymond, *Inorg. Chem.* **2000**, *39*, 2652-2660.

[48] P. Gans, A. Sabatini, A. Vacca, *Talanta* **1996**, *43*, 1739-1753.

[49] P. Gans, A. Sabatini, A. Vacca, *HYPERQUAD2003*; University of Leed and University of Florence: Leeds, U.K., and Florence, Italy, 2003.

[50] P. Gans, A. Sabatini, A. Vacca, *Annali Di Chimica* **1999**, *89*, 45-49.

[51] P. L. Brown, *Radiochimica Acta* **2002**, *90*, 589-93.

[52] L. Alderighi, P. Gans, A. Ienco, D. Peters, A. Sabatini, A. Vacca, *Coord. Chem. Rev.* **1999**, *184*, 311-318.

[53] P. Gans, *HySS2; University of Leeds, Leeds, U.K., 2000*.

Scheme and Figure Legends:

Figure 1. Mono- and bis-bidentate Me-3,2-HOPO ligands previously studied.[34-36]

Figure 2. Water-soluble bis-Me-3,2-HOPO ligands.

Figure 3. Ligand L^9H_2 and two views of the crystal structure of its uranyl complex $UO_2(L^9)(DMSO)$. Thermal ellipsoids are drawn at the 50% probability level. Hydrogen atoms and non-coordinating solvent are omitted for clarity. Oxygen atoms are red, carbons gray, nitrogens blue, sulfur yellow, and uranium silver.

Figure 4. Intramolecular stabilization of deprotonated Me-3,2-HOPO ligands.

Figure 5. Representative reversibilities of uranyl titrations with bis-Me-3,2-HOPO ligands through pH 11: L^3H_2, (left, reversible) and L^6H_2, (right, irreversible).

Scheme 1. Intramolecular hydrogen bonding in bis-Me-3,2-HOPO ligands upon deprotonation/metalation.

Scheme 2. Formation of a $[UO_2L(OH)]^-$ species. Uranyl oxo atoms are omitted for clarity.

Scheme 3. Proposed speciation of uranyl titrations with L^6H_2. Uranyl oxo atoms are omitted for clarity.

Scheme 4. Proposed speciation of uranyl titrations with L^1H_2. Uranyl oxo atoms are omitted for clarity.

Table 1. Crystallographic parameters for $UO_2(L^9)(DMSO)$.

Formula	$C_{28}H_{34}N_4O_{11}SU \cdot \frac{1}{4}H_2O$	**Cryst. size [mm^3]**	$0.35 \times 0.10 \times 0.05$
MW	877.19	T **[K]**	115(2)
Crystal system	Orthorhombic	Z	8
Space group	*Pbca*	ρ_{calcd} **[g·cm^{-3}]**	1.923
Habit	Plate	μ_{palcd} **[mm^{-1}]**	5.494
Color	Red	θ_{min}, θ_{max}, **[°]**	3.29, 26.36
a **[Å]**	13.451(2)	**Total reflections**	27837
b **[Å]**	15.839(2)	**Data/ restr./ param.**	5978 / 0 / 410
c **[Å]**	28.445(4)	$F(000)$	3428
α **[°]**	90	T_{min}/T_{max}	0.324
β **[°]**	90	$R1[I>2\sigma(I)]^{[a]}$	0.0304
γ **[°]**	90	**wR2(all data)**[a]	0.0738
V **[Å^3]**	6060.3(16)	**GOF**[a]	1.040

[a] $R1 = \Sigma||F_o| - |F_c||/\Sigma|F_o|$; $wR2 = [\Sigma[w(F_o^2 - F_c^2)^2]/\Sigma[w(F_o^2)^2]]^{1/2}$; $GOF = [\Sigma w(|F_o| - |F_c|)^2/(n - m)]^{1/2}$

Table 2. pK_a values of bis-Me-3,2-HOPO ligands.

Ligand	n[a]	pK_{a1}	pK_{a2}	ΣpK_a
L^1H	--	6.12[42]	--	--
2Li-Me-3,2-HOPO	2	5.82(3)	6.68(3)	12.50(4)
4Li-Me-3,2-HOPO	4	6.01(1)	7.02(4)	13.03(4)
L^2H_2	2	5.10(6)	6.45(1)	11.55(6)
L^3H_2	3	5.37(2)	6.72(2)	12.09(3)
L^4H_2	4	5.25(4)	6.60(3)	11.85(5)
L^5H_2	5	5.52(7)	6.75(2)	12.27(7)
L^6H_2	2	4.91(8)	6.22(1)	11.13(8)
L^7H_2	2	5.09(3)	6.29(1)	11.38(3)
L^8H_2	5	5.70(6)	6.75(2)	12.45(6)

[a] n = number of carbon atoms between amide nitrogens.

Table 3. Log β_{mlh} values for uranyl titrations with Me-3,2-HOPO ligands.

Ligand	log $\beta_{11\text{-}2}$	log $\beta_{11\text{-}1}$	log β_{110}	log $\beta_{12\text{-}1}$	log β_{120}	log $\beta_{22\text{-}1}$	log $\beta_{22\text{-}1}$	log β_{220}
L^1H[a]	-2.50(6)		10.64(3)	11.48(4)	17.91(2)			
L^2H_2		6.30(8)	12.5(1)					
L^3H_2		5.86(6)	12.6(1)					
L^4H_2		6.97(6)	13.9(1)					
L^5H_2		5.64(4)	13.42(7)					
L^6H_2[a]						15.74(5)	22.47(8)	28.1(1)
L^7H_2		6.6(1)	13.04(1)					
L^8H_2[a]		5.38(5)	12.89(1)					

[a] In addition to low pH data (pH 3 to pH 1.6), only forward (acid to base) titration data was used due to observed irreversibility

Table 4. Calculated pUO_2 values for Me-3,2-HOPO ligands.

Ligand	pUO_2[a]		
	pH 2.5	pH 7.4	pH 8.5
L^1H	7.98(3)	14.70(4)	15.96(3)
L^2H_2	7.0(1)	14.63(8)	15.75(8)
L^3H_2	6.6(1)	14.24(7)	15.34(6)
L^4H_2	8.0(1)	15.39(7)	16.43(9)
L^5H_2	7.1(1)	14.44(6)	15.16(4)
L^6H_2	6.01(1)	13.39(3)	14.48(2)
L^7H_2	7.62(4)	14.97(9)	16.1(1)
L^8H_2	6.55(6)	14.00(3)	14.87(5)

[a] $pUO_2 = -\log[UO_2{}^{2+}{}_{free}]$, $[UO_2{}^{2+}] = 1$ μM, $[L] = 10$ μM

TOC Text:
Catch Phrase: Bis-Me-3,2-HOPO Uranyl Affinity
Text: Seven water-soluble, tetradentate, bis-Me-3,2-HOPO ligands were synthesized and their affinity for the uranyl cation determined by solution phase titrations. The butyl-linked ligand exhibits the greatest uranyl affinity at all pH, with the rigid *o*-phenylene-linked ligand displaying the next highest affinity of the ligands investigated. No discernable trends in uranyl affinity could be identified in relation to linker length or geometry.

Figure 1

Figure 2

L^9H_2

Figure 3

Figure 4

Figure 5

Scheme 1

Scheme 2

Scheme 3

Scheme 4

LEGAL DISCLAIMER